Non-linear fracture mechanics, a novel approach for quasi-brittle materials

E. Morice, S. Pommier, A. Delaplace

LMT, École Normale Supérieure de Cachan, Cachan (France)
morice@lmt.ens-cachan.fr

ABSTRACT. Crack growth in non-linear quasi-brittle materials is addressed by a new approach. This approach is consistent with the Linear Elastic Fracture Mechanics framework ; the velocity field around the crack tip is represented by a sum of shape functions and their intensity factors. However, the LEFM kinematics is enriched to account for the non-linear behaviour of the material. Additional shape functions and their intensity factors are used to capture the effect of the nucleation of micro-cracks on the crack tip fields. So as to construct these shape functions, a multi-scale approach is employed. The discrete element method is used to compute the velocity field around a crack tip with boundary conditions extracted from finite element simulations. The results are post-treated using a proper orthogonal decomposition to generate additional shape functions for mode I and mode II loading conditions. Once this is done, the evolution of crack tip damage during a complex loading scheme is condensed into the evolutions of the intensity factors of the two additional shape functions.

KEYWORDS. Quasi-brittle material, non-linear fracture mechanics, discrete element method, damage, crack

INTRODUCTION

Being able to accurately predict the leakage rate through a cracked or damaged concrete shell remains a major challenge to nuclear safety. It requires accounting explicitly for the presence of cracks and for crack opening, sliding and growth. However, linear elastic facture mechanics fails to model the permeability of cracked concrete shells. As a matter of fact, concrete and mortar display a non-linear behaviour because of their quasi-brittle nature. The crack tip process zone consists in a high number of micro-cracks among which some coalesce to promote macroscopic crack growth and others produce a shielding effect to the macro-crack.
The discrete element method (DEM) is attractive to deal with this type of problems. The quasi-brittle material is modelled as a Voronoï tessellation of particles and a set of connections between them. The connections are modelled as cohesive forces. This first study is focused on tension loadings. At this stage, contact and friction forces can thus be neglected. The maximum allowable strain in each connection is statistically distributed so as to represent the heterogeneity of the material. The process of micro cracking is then described by the breaking of connections between particles and generates naturally the appropriate complexity (damage localization, cracks pattern formation, etc.).
Nevertheless, modelling the behaviour of a nuclear core concrete shell by the DEM remains up to now out of reach. The aim of this study is thus to enrich the usual fracture mechanics framework so as to account for the quasi-brittle behaviour of the material. For this purpose, a scaling method is used to benefit from discrete element method simulations capabilities to build a non-linear fracture mechanics model.
Instead of using classical LEFM fields to represent the velocity field, it was chosen to enrich the kinematics of the crack tip region by adding additional field that stand for micro cracking and damage. As in LEFM, these fields are expressed as the product of an intensity factor and of a shape function. The shape functions are defined a priori and are solely function

of space. The intensity factors are functions of time. In I+II mixed mode conditions, the evolutions of 4 intensity factors, a linear and a non-linear one for each mode thus fully characterize the behaviour of the crack tip region. The discrete element method [1] is used to compute velocity field evolutions that are post-treated to generate evolutions of the four intensity factors during complex I+II mixed mode loading schemes.

DISCRETE MODEL

In the considered discrete model [1], the material is described as a Voronoï particle assembly, representative of the material heterogeneity. A grid support is used for generated Voronoï particle centre in order to easily control mesh variability and to simplify the application of boundary conditions. Basically two types of interactions are considered, cohesive and contact force, however our study focuses only on tension loading, so we'll consider only cohesive forces.

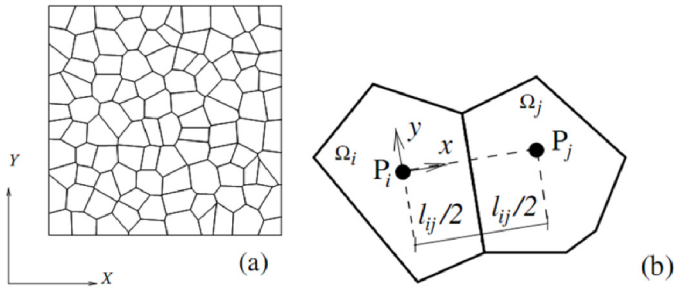

Figure 1: Discrete model (a) and representation of Voronoï cells and their connections (b).

Cohesive forces

Interactions are limited to cohesive forces. Each particle has 3 degrees of freedom (2 in translations and 1 in rotation), and a 6 x 6 local stiffness matrix is adequate to represent the complete interaction. Following Schlangen and Garboczi [4], Van Mier et al. [5], an Euler-Bernoulli beam matrix is used in the model to connect each pair of neighbouring particles *i* and *j*.

Non-linear behaviour

Considering a perfectly elastic behaviour for the beams renders damage evolution. The breaking criterion for a connection P_{ij} between two particles i and j, is function of the strain ε_{ij} of the beam used as a connector and of the rotation values θ_i and θ_j of particles i and j:

$$P_{ij} = \left(\frac{\varepsilon_{ij}}{\varepsilon_{cr}}\right)^2 + \left(\frac{\max\left(|\theta_i|,|\theta_j|\right)}{\theta_{cr}}\right)^2 \geq 1 \qquad (1)$$

ε_{cr} and θ_{cr} are two material parameters, the first one controlling essentially the tensile behaviour of the discrete model, and the second its compressive behaviour. These two parameters are statistically distributed so as to account for the heterogeneity of the material.

BOUNDARY CONDITIONS

Computations with the discrete elements method are driven in displacement. The displacement applied on the faces of the discrete model comes from a linear elastic finite element simulation. This method is used for various mode I + II mixed mode loading schemes. The finite element model corresponds to a 1m x 1m square plate with a centre crack with a length 2a = 100 mm. The area analysed using the discrete element method is a 12mm x 12mm square having the crack tip in its centre at the beginning of the calculation. The discrete element mesh was constructed so as to display a symmetry plane along the crack plane.

CRACK TIP FIELDS ANALYSIS IN MODE I & II LOADING CONDITIONS

Partition hypothesis

At this stage, the velocity field computed using the discrete element method is analysed to extract its main characteristics. First of all, it is aimed at building a model consistent with the fracture mechanics framework. The crack is thus modelled by a local plane and front, which makes possible defining a local axis system R_T. The velocity field of a point P in the crack tip region can then be calculated as:

$$v(P,t)_{R_0} = v(T,t)_{R_0} + \omega(R_T / R_0) \wedge \underline{TP} + v(P,t)_{R_T} \tag{2}$$

Where R_0 is the axis system of the model. In this equation, the first part stems from crack growth and deviation and the second part $v(P,t)_{R_T}$ is the velocity field within the axis system attached to the crack tip T. For the sake of simplicity $v(P,t)_{R_T}$ will be denoted by $v(P,t)$ in the following.

The Mode I being symmetric and mode II anti-symmetric with respect to the crack plane and to the crack front, $v(P,t)$ is then partitioned as followed into mode I and mode II part :

$$v(P,t) = v_I(P,t) + v_{II}(P,t) \tag{3}$$

Where the mode I and II parts are then calculated as:

$$\begin{aligned} v_I^x(x,y,t) &= \frac{v_I^x(x,y,t) + v_I^x(x,-y,t)}{2} \quad & v_{II}^x(x,y,t) &= \frac{v_{II}^x(x,y,t) - v_{II}^x(x,-y,t)}{2} \\ v_{II}^x(x,y,t) &= \frac{v_{II}^x(x,y,t) - v_{II}^x(x,-y,t)}{2} \quad & v_{II}^y(x,y,t) &= \frac{v_{II}^y(x,y,t) + v_{II}^y(x,-y,t)}{2} \end{aligned} \tag{4}$$

The second step is to approximate the crack tip velocity field by a sum of products of shape functions and of intensity factors. For each fracture mode, a "linear elastic" shape function is first introduced to be consistent with the LEFM framework. Then an additional shape function is constructed to carry the non-linear behaviour of the crack tip process zone induced by the presence of micro-cracks.

Linear elastic shape functions

Linear elastic reference fields u_e^I and u_e^{II} are obtained from elastic simulations using the discrete model. Boundary conditions in displacement are provided by finite element simulations respectively in mode I and II from which the displacement field is extracted. In order to model a linear elastic response with the discrete element model, the connections between particles are all considered as unbreakable. The linear elastic reference field is then obtained after partitioning into mode I and mode II components the displacement field computed by the discrete element method.

Construction of the additional shape functions

To obtain the two additional fields, the discrete element model is loaded either in mode I or in mode II. The connections between particles are now allowed to break. The solution $v(P,t)$ of a monotonic loading case computed using the discrete element method is post-treated by an orthogonal decomposition algorithm. First, the velocity field $v(P,t)$ is projected onto the linear elastic reference fields. The projection onto u_e^I (resp. u_e^{II}) is denoted $\dot{\tilde{K}}_I$ (resp. $\dot{\tilde{K}}_{II}$). $\dot{\tilde{K}}_I$ (resp. $\dot{\tilde{K}}_{II}$) can slightly differ from the rate of the nominal applied stress intensity factor $\dot{K}_I^\infty$ (resp. $\dot{K}_{II}^\infty$). As a matter of fact, two types of stress can generate a "linear-elastic" response, the macroscopic stress field and the internal stress field, which can arise, for instance, from the shielding effect of micro-cracks within the process zone.

$$\dot{\tilde{K}}_I = \frac{\int_{r=0}^{r_{\max}} \int_{\theta=-\pi}^{\pi} v(P,t).u_e^I(P) r d\theta dr}{\int_{r=0}^{r_{\max}} \int_{\theta=-\pi}^{\pi} u_e^I(P) \cdot u_e^I(P) r d\theta dr} \tag{5}$$

The residue is then calculated:

$$v^{res}(P,t) = v(P,t) - \dot{\tilde{K}}_I(t)u_e^I(P) \tag{6}$$

This residue can be decomposed in a sum of a product of spatial field, mutually orthogonal, and their intensity factors using the Karhunen-Loeve transform [3]. We only keep the first term $u_c^I(P)$ of this decomposition for each mode.

$$v^{res}(P,t) = \sum_{m=1}^{m_0} \dot{a}_m(t)u^m(P) \tag{7}$$

We will then assume that the two linear elastic reference fields u_e^I and u_e^{II} and the two additional fields u_c^I and u_c^{II} that were constructed using either linear elastic or non-linear conditions for monotonic mode I or mode II loading phases can be used to represent any complex mixed mode loading scheme. With this approximation:

$$v(P,t) \approx \tilde{v}(P,t) = \dot{\tilde{K}}_I(t)u_e^I(P) + \dot{\tilde{K}}_{II}(t)u_e^{II}(P) + \dot{\rho}_I(t)u_c^I(P) + \dot{\rho}_{II}(t)u_c^{II}(P) \tag{8}$$

This assumption is valid only if the process zone is confined inside an elastic bulk that controls and limits the movement inside the process zone. The Karhunen-Loeve transform was selected because it uses the self-correlation matrix of the movement. In other words, it partitions the movement inside the process zone into uncorrelated or independent movements. As a consequence, the intensity factors represent the independent degrees of freedom of the process zone.

With this hypothesis, the evolution of the four intensity factors $\left(\dot{\tilde{K}}_I, \dot{\tilde{K}}_{II}, \dot{\rho}_I, \dot{\rho}_{II}\right)$ of the four reference fields $\left(u_e^I, u_e^{II}, u_c^I, u_c^{II}\right)$ is a condensed measure of the non-linear behaviour of the process zone. To verify the quality and the suitability of that hypothesis, the error associated to the approximation of the velocity field is calculated at each time step.

Extraction of the intensity factors

Having at our disposal an orthogonal basis of spatial reference fields $\left(u_e^I, u_e^{II}, u_c^I, u_c^{II}\right)$, defined a priori for a given material, makes possible to project the velocity field $v(P,t)$, obtained for any loading sequence, onto this basis.

First the rate of the mode I (resp. mode II) linear-elastic intensity factor $\dot{\tilde{K}}_I$ (resp. $\dot{\tilde{K}}_{II}$) is extracted as shown in Eq. 5. This rate is given in $MPa\sqrt{m}\cdot s^{-1}$ and is very close the rate of the nominal applied stress intensity factor K_I^∞ (resp. K_{II}^∞). We then proceed as follows to extract the rate of the mode I (resp mode II) non-linear intensity factor $\dot{\rho}_I$ (resp $\dot{\rho}_{II}$):

$$\dot{\rho}_I = \frac{\int_{r=0}^{r_{\max}} \int_{\theta=-\pi}^{\pi} v(P,t).u_c^I(P) r\,d\theta\,dr}{\int_{r=0}^{r_{\max}} \int_{\theta=-\pi}^{\pi} u_c^I(P).u_c^I(P) r\,d\theta\,dr} \tag{9}$$

Error calculation

Once the four intensity factors are extracted, an approximation $\tilde{v}(P,t)$ of the computed velocity field $v(P,t)$ is provided in Eq. (8). It is useful to define two errors associated with this approximation:

- the error $C_1(t)$, associated with a linear elastic representation of the velocity field
- the error $C_2(t)$, associated with a non-linear representation of the velocity field.

The error $C_1(t)$ and the relative error $C_{1R}(t)$ are calculated as follows:

$$C_1(t) = \sqrt{\int_D \left(v(P,t) - \dot{\tilde{K}}_I(t)u_I^e(P) - \dot{\tilde{K}}_{II}(t)u_{II}^e(P)\right)^2 dv}, \quad C_{1R}(t) = C_1(t) \Big/ \sqrt{\int_D (v(P,t))^2\, dv} \tag{10}$$

The error $C_2(t)$ and the relative error $C_{2R}(t)$ are calculated as follows:

$$C_2(t) = \sqrt{\int_D \left(v(P,t) - \tilde{v}(P,t)\right)^2 dv}, \quad C_{2R}(t) = C_2(t) \Big/ \sqrt{\int_D (v(P,t))^2\, dv} \tag{11}$$

These errors will indicate us if the approach is valid and the difference between C_{1R} and C_{2R} will indicate us whether or not a non-linear approach is really needed, or in other word, when the process zone behaviour can be considered as having a linear-elastic behaviour or not.

ADDITIONNAL FIELDS

R-dependency

To illustrate this method, the additional fields, u_c^I and u_c^{II}, obtained by a proper orthogonal decomposition, were post-treated a second time so as to partition them into a function of the distance to the crack tip r and of the angular location θ.

$$u_c^I(P) \approx g_c^I(r) f_c^I(\theta) \quad \text{and} \quad u_c^{II}(P) \approx g_c^{II}(r) f_c^{II}(\theta) \tag{12}$$

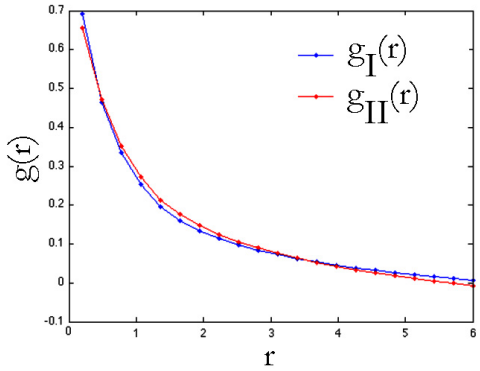

Figure 2: Comparison of r-dependence between mode I and II, r-components.

In Fig.2, the r-dependency of the additional field is presented for each mode. That dependency is very similar for the two modes. The evolution appears to be roughly proportional to r^{-1}. It is expected that this dependency is function of the distribution function chosen for the fracture threshold of the connections between particles.

θ-dependency

Since the θ-shape function $f_c^{I\ or\ II}(\theta)$ has two components (a radial and a hook ones), it was chosen to represent it using the deformation of an initial circle induced by either the mode I (Fig. 3a) or the mode II (Fig. 3b) θ-shape function $f_c^{I\ or\ II}(\theta)$ of the additional fields. In both cases, there is a discontinuity of the velocity field along the crack plane, the mode I component being symmetric and the mode II anti symmetric.

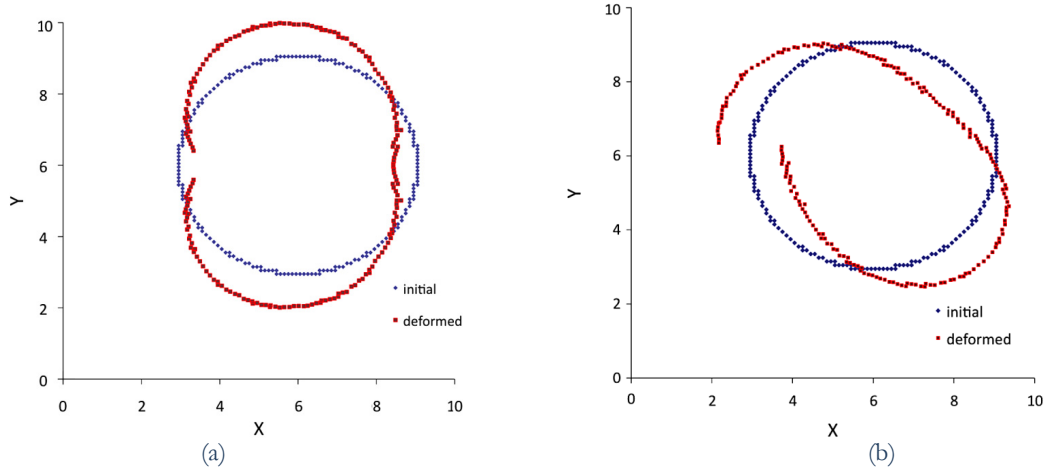

Figure 3: Dependency in θ of the complementary field in mode I (a) and II (b).

The opening of the circle ends in mode I, analogous to a CTOD, is interesting to make the mode I additional field in dimensionless.

For the deformed circle in mode II, the displacement of the point in θ=- π and θ=π, are of opposite sign, which is consistent with an anti-symmetric mode of fracture. This gap, analogous to a CTSD, can be useful to make the mode II additional field in dimensionless.

INTENSITY FACTORS EVOLUTIONS

Computations have been made for mode I and II cyclically increasing loading cycles. For each time increment, the velocity field computed using the discrete elements method is projected onto the basis of reference field that was constructed using previous calculations. Then the intensity factors extracted from each loading sequence can be plotted as a function of the nominal applied stress intensity factor.

In Fig. 4, (a) and (c) the difference between $\widetilde{K}_I$ and K_I^∞ (resp. $\widetilde{K}_{II}$ and K_{II}^∞) is plotted against the nominal applied stress intensity factor K_I^∞ (resp. K_{II}^∞). First of all it can be seen that there is nearly a factor 200 between K_I^∞ and $\widetilde{K}_I - K_I^\infty$. In the following this difference will then be neglected, the intensity of the linear elastic field can be considered as the nominal applied stress intensity factor for each mode, though a slight difference is observed, that is interpreted as a shielding effect induced by micro-cracks in the process zone ($\widetilde{K}_I < K_I^\infty$). From these calculations, this shielding effect is quite small. In addition, it is observed that this shielding effect is decreasing when the loading level increases and when new connections are broken.

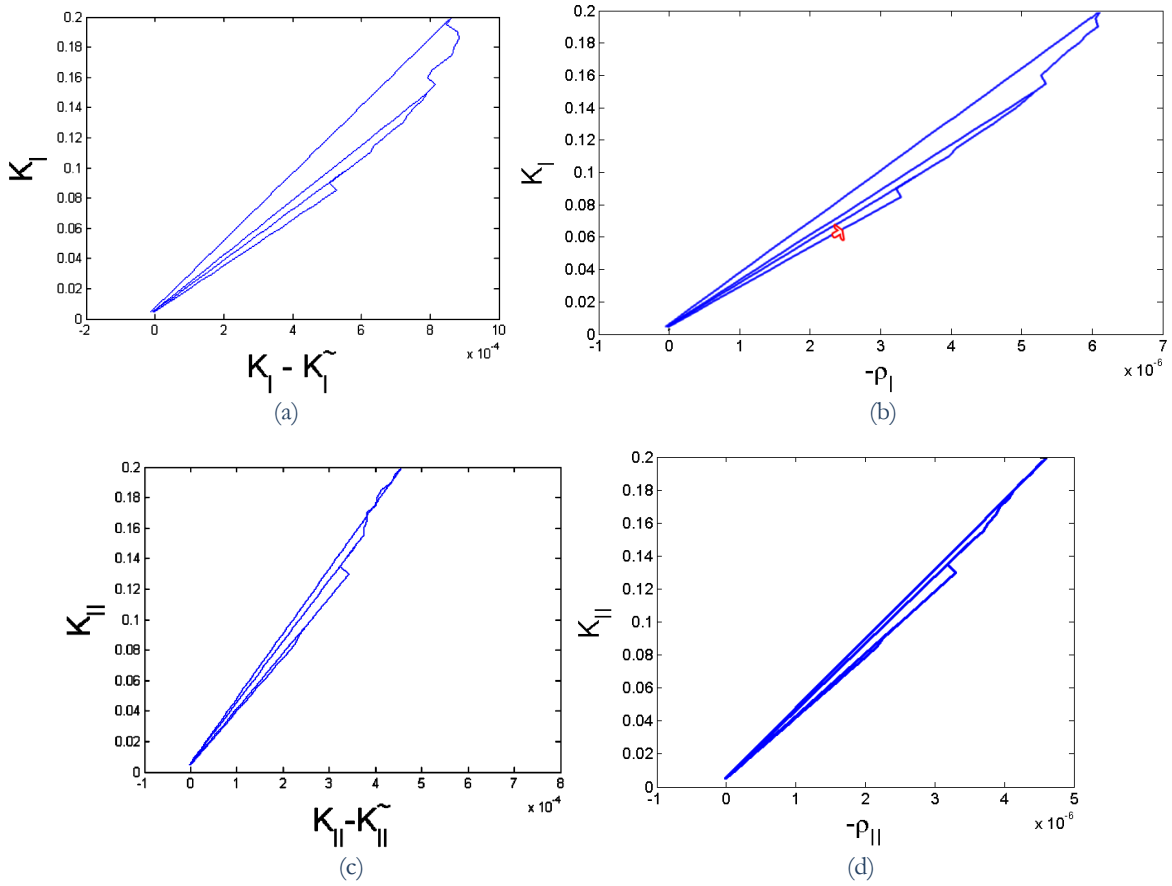

Figure 4: Evolution of linear-elastic and non-linear intensity factors with the stress intensity factor in mode I ((a), (b)) and in mode II ((c), (d)). In Fig 4 (c) an arrow indicates the first loading ramp.

In Fig. 4 (b) and (d), the non-linear intensity factor ρ_I (resp. ρ_{II}) is plotted against the nominal applied stress intensity factor K_I^∞ (resp. K_{II}^∞). It is clear in this graph that ρ_I (resp. ρ_{II}) does not represent directly the damage of the process zone. In fact, ρ_I (resp. ρ_{II}) represent the contribution of micro-cracks to the velocity field in the process zone. When the process zone is loaded of unloaded below the maximum value of K_I^∞ reached during previous cycles, there is no longer break of connections. In other word, there is no micro-crack creation within the process zone. In this case, we first observe that the K_I^∞ - ρ_I curve is a straight line and that its slope is constant. We also observe that the two errors C_{1R} and C_{2R} are both very small. During such loading and unloading phases existing micro-cracks do cyclically close and open.
It is important to notice that ρ_I is negative. As a matter of fact, the presence of micro-cracks ahead of the tip of the macro-crack is producing a shielding effect that can be expressed as a negative correction to the LEFM field. In fact, provided that the spatial distribution and the density of micro-cracks was known, conventional analytical methods (such as the distributed dislocation technics [6]) would allow calculating the exact solution for the velocity field in presence of micro-cracks and determine precisely that shielding effect.

However, when new micro-cracks are created (when connections are broken) the slope of the K_I^∞ - ρ_I curve changes. In addition, we observe that both C_{1R} and the difference between C_{1R} and C_{2R} increase significantly during loading phases for which connections are broken (in any cases, it is found that C_{2R} is small, well below 0.1%).

The damage of the process zone is related to the slope of the K_I^∞ - ρ_I curve during loading phases for which no micro-cracks are created. The evolution law of damage is given by the variation of that slope during loading.

The most interesting result is that in Fig. 4 (b) and (d) the slope of the K_I^∞ - ρ_I curve increases when the amount of broken connections is increasing. In this first analysis we did not try to load the model above 0.2 MPa.m$^{1/2}$, however, we can see that which indicates that the shielding effect of micro-cracks is progressively decreasing when the micro-cracks density is increasing.

CONCLUSION

An enriched kinematic is proposed to represent the crack tip field in quasi-brittle materials. A basis of reference fields was constructed once for all for a given material. It contains a linear-elastic and a non-linear field for each mode. During a complex loading scheme, the velocity field in the process zone computed using the discrete element method, is projected onto this basis so as to extract the intensity factors.
The behaviour of the crack tip region can then be analysed through the evolutions of the four intensity factors of the four reference fields. For each mode, the intensity factor of the elastic-linear reference field is extremely close to the nominal applied stress intensity factor.
The intensity factors of the non-linear reference fields represent the contribution of micro-cracks to the movement in the process zone for each mode. This contribution is negative, which indicates a shielding effect of micro-cracks on the macro-crack. The results show also that this shielding effect decreases progressively when the damage of the process zone increases (more connection are broken), the same phenomenon is observed for each mode
The next step is to determine the relation between the material parameter (distribution of ε_{cr} and θ_{cr}) on the reference fields (r-dependency and q-dependency).
Then our aim is to use the discrete element method to generate curves as those plotted in Fig. 4 (b) and (d) and to use these curves to identify a non-linear constitutive model for fracture mechanics that would allow better predictions of the behaviour of cracks in quasi-brittle materials.

REFERENCES

[1] A. Delaplace, Geomech. Geoengng., 4 (1) (2009) 79.
[2] S. Pommier, R. Hamam, Fatigue Fract. Engng Mater. Struct., 30(7) (2007) 582.
[3] K. Karhunen, Mat.-Phys., 37 (1947) 1.
[4] E. Schlangen, E. J. Garboczi, Eng. Fract. Mech., 57(1997) 319.
[5] J. G. M. Van Mier, M. R. A. Van Vlietn T. K. Wang, Mech. Mater., 34 (2002) 705.

[6] D. A. Hills, P. A. Kelly, D. N. Dai, A. M. Korsunsky, Solution of Crack Problems, The Distributed Dislocation Technique, Kluwer Academic Pub., Dordrecht (1996).